INTERVENTIONAL RADIOLOGY
Official journal of the Japanese Society of Interventional Radiology and Asia Pacific Society of Cardiovascular and Interventional Radiology

TECHNICAL NOTE

Optimal Virtual-target Definition for Detecting Feeding Arteries of Renal Cell Carcinoma Using Automated Feeder-detection Software

Soichiro Okamoto[1)], Yusuke Matsui[2)], Takahiro Kawabata[3)], Koji Tomita[1)], Kazuaki Munetomo[1)], Noriyuki Umakoshi[1)], Fumiyo Higaki[1)], Toshihiro Iguchi[4)] and Takao Hiraki[2)]

1) Department of Radiology, Medical Development Field, Okayama University, Japan
2) Department of Radiology, Faculty of Medicine, Dentistry and Pharmaceutical Sciences, Okayama University, Japan
3) Department of Radiology, Tsuyama Chuo Hospital, Japan
4) Department of Radiological Technology, Faculty of Health Sciences, Okayama University, Japan

Abstract:
Purpose: To determine the optimal virtual-target definition for detecting renal cell carcinoma feeders using transarterial computed tomography angiography with automated feeder-detection software.
Material and Methods: This retrospective study included 17 patients with 17 renal cell carcinomas who underwent transarterial ethiodized-oil marking before cryoablation. Tumor feeders were automatically detected on transarterial renal computed tomography angiography images using the automated feeder-detection software with three virtual-target definitions: small (ellipsoidal area maximized within the tumor contour), medium (ellipsoidal area covering the entire tumor with a minimal peripheral margin), and large (ellipsoidal area including the tumor and a 5-mm peripheral margin). The detected feeders were classified as true or false positives according to the findings of selective renal arteriography, by consensus of two interventional radiologists. Feeder-detection sensitivity and the mean number of false-positive feeders per tumor were calculated for each virtual-target definition.
Results: For 17 tumors, 25 feeding arteries were identified on the arteriography. The feeder-detection sensitivity of the software was 80.0% (20/25), 88.0% (22/25), and 48.0% (12/25) for small, medium, and large virtual targets, respectively. The mean ± standard deviation number of false-positive feeders per tumor was 0.82 ± 1.3, 1.41 ± 1.1, and 2.82 ± 1.6 when using small, medium, and large virtual-target definitions, respectively.
Conclusions: The detection rate of renal cell carcinoma feeders with the automated feeder-detection software varies according to the virtual-target definition. Using a medium virtual target, covering the entire tumor with a minimal peripheral margin, may provide the highest sensitivity and an acceptable number of false-positive feeders.

Keywords:
computed tomography angiography, kidney, software, therapeutic embolization

Interventional Radiology 2025; 10: e2025-0034
https://doi.org/10.22575/interventionalradiology.2025-0034
https://ir-journal.jp/

Introduction

Transarterial ethiodized-oil marking facilitates tumor visualization during CT-guided renal cell carcinoma (RCC) ablation, possibly enhancing local therapeutic efficacy [1-4]. Accurate detection and superselective catheterization of the feeding arteries are required for successful tumor marking while minimizing damage to the surrounding renal parenchyma. However, identifying RCC feeders using conventional DSA can be challenging because of the complex renal vascular anatomy [5].

Using automated feeder-detection (AFD) software with CTA helps identify hepatic and renal tumor feeders in transarterial therapies [6, 7]. The software identifies potential feeders on CTA images based on the catheter-tip position and a manually defined virtual target corresponding to the tumor. Feeder detectability may vary with the virtual-target definition, as shown in a previous study that compared three definitions for detecting HCC feeders [8]. However, the optimal virtual-target definition for detecting RCC feeders re-

Corresponding author: Yusuke Matsui, y-matsui@okayama-u.ac.jp
Received: May 31, 2025, Accepted: September 1, 2025, Published: October 31, 2025

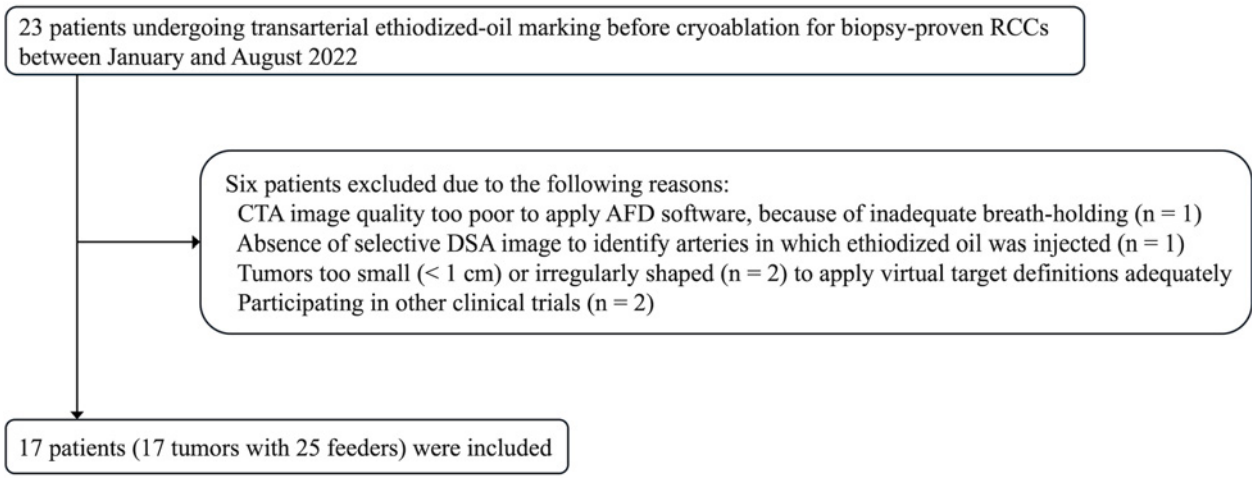

Figure 1. Flow chart of the patient selection process.
RCC: renal cell carcinoma

mains unclear.

Herein, we investigated the optimal virtual-target definition for detecting RCC feeders using the AFD software.

Material and Methods

Study population

This study was approved by the relevant institutional review board. Opt-out consent was obtained for retrospective patient data use.

Patients who underwent transarterial ethiodized-oil marking before cryoablation for biopsy-proven RCC between January and August 2022 were included. Patients were excluded if i) CTA image quality was too poor to apply AFD software because of inadequate breath holding; ii) the artery in which ethiodized oil was injected could not be identified because of lack of selective DSA images; iii) the tumors were too small (< 1 cm) or irregularly shaped to adequately apply virtual-target definitions, and iv) they participated in other clinical trials. Seventeen patients with 17 RCCs were included in the study (**Figure 1**).

Transarterial ethiodized-oil marking

All procedures were performed using a hybrid angio-CT suite equipped with an angiographic C-arm and a 320-row CT scanner (Aquilion ONE; Canon Medical Systems, Otawara, Japan). A 4-Fr catheter was inserted into the renal artery using the femoral approach. Transarterial renal CTA was performed using contrast medium (300 mg I/mL) diluted 1:2 with saline. Two-volume scans were performed at 1.0 and 5.0 s after initiating contrast injection (3.0 mL/s for 5 s) using the following parameters: 120-kV tube voltage, automatic exposure control for tube current, 160-mm beam width, 1.0-s rotation times. A deep-learning algorithm (AiCE; Canon Medical Systems) was used for image reconstruction. Subsequently, renal arteriography was performed, and tumor feeders were selected using a 1.7- or 1.9-Fr microcatheter. After confirming tumor staining with selective DSA, ethiodized oil was injected. Gelatin sponge particles were injected at the operator's discretion. The procedural endpoint was complete ethiodized-oil deposition (i.e., deposition throughout the entire tumor), which was confirmed using CT.

Analysis of automated feeder detection using the software

The AFD software (Embolization Plan in Alphenix Workstation version 9.0; Canon Medical Systems) was retrospectively applied to the transarterial renal CTA images of each patient. A radiological technologist (12 years of experience), supervised by a board-certified interventional radiologist, delineated virtual targets on second-phase images using three definitions [8]: small (ellipsoidal area maximized within the tumor contour), medium (ellipsoidal area covering the entire tumor with a minimal peripheral margin), and large (ellipsoidal area including the tumor and a 5-mm peripheral margin) (**Figure 2**). Ellipsoidal segmentation was adopted to enhance clinical applicability, as freeform contouring along the tumor boundaries could be time-consuming and less practical in time-constrained clinical settings. It was also considered less dependent on the individual performing the segmentation, potentially contributing to improved reproducibility.

The virtual target was superimposed on the first-phase images for software-based tumor-feeder detection. The software-detected vessels were classified as true- or false-positive feeders by two interventional radiologists (14 and 12 years of experience), in consensus, referring to DSA and CTA images. True-positive feeders were defined as software-detected vessels that matched the specific arterial branch into which the ethiodized oil was injected via microcatheter during the marking procedures. In contrast, any vessels demonstrated by the software that did not receive ethiodized oil injection were classified as false-positive feeders (**Figure 3**). When the software partially visualized a true feeder vessel, without identifying the specific distal branch into which the ethiodized oil was injected, the detected vessel was excluded from both true- and false-positive counts. This approach was

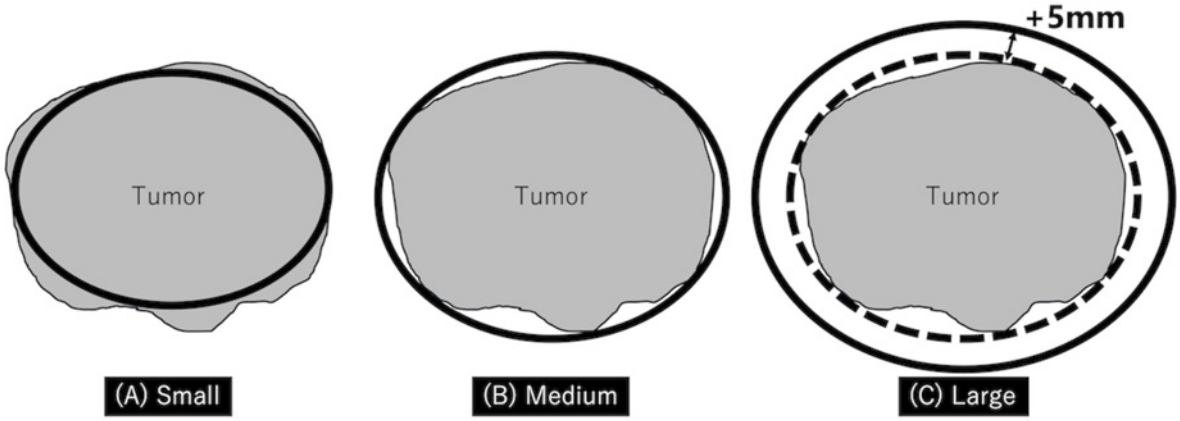

Figure 2. Schema illustrating the three virtual-target definitions.
(A) Small: ellipsoidal area maximized within the tumor contour; (B) Medium: ellipsoidal area covering the entire tumor with a minimal peripheral margin; and (C) Large: ellipsoidal area including the tumor and a 5-mm peripheral margin. The thick black circle represents the boundary of each virtual target. The dotted circle in (C) represents the tumor margin.

adopted to enable a rigorous evaluation of the software's ability to accurately identify the specific arterial branch where the microcatheter tip needs to be positioned for ethiodized-oil injection.

Statistical analysis

Continuous data are summarized as mean and standard deviation (SD). Categorical variables are described using raw numbers and percentages. The feeder-detection sensitivity (%) was calculated for each virtual-target definition by dividing the number of true-positive feeders by the total number of treated feeders. The mean ± SD number of false-positive feeders per tumor was calculated for each definition. Statistical analyses were performed using EZR v.1.68 (Saitama Medical Center, Jichi Medical University, Saitama, Japan) [9].

Results

For the 17 tumors, 25 feeders were identified. **Table 1** summarizes the patient and tumor characteristics. Complete ethiodized-oil deposition was confirmed in all 17 tumors (100%). The feeder-detection sensitivity of the software was highest for the medium (88.0% [22/25]), followed by the small (80.0% [20/25]) and the large virtual target (48.0% [12/25]) (**Table 2**). Overall, 14, 24, and 48 false-positive feeders were detected for 17 tumors when using small, medium, and large virtual-target definitions, respectively. The mean number of false-positive feeders per tumor was 0.82 ± 1.3, 1.41 ± 1.1, and 2.82 ± 1.6 when using the small, medium, and large virtual-target definitions, respectively (**Table 2**). Although the seven vessels demonstrated with the large virtual-target definition were consistent with the middle of the feeder pathway, the distal branches selected using the microcatheter were not detected, as they were included within the areas of the virtual targets. Such vessels were not counted as true or false-positive feeders. Three tumor feeders in two patients were undetected using any of the target definitions. One was a minor feeder (ϕ 0.5 mm) from the renal capsular artery. The remaining two feeders were undetected because the software could not correctly trace the vascular continuity in the proximal renal artery.

Discussion

In this study, the AFD software with a medium virtual-target definition demonstrated the highest sensitivity (88.0%) for detecting RCC feeders. As the size of the virtual target increased, the number of false-positive feeders increased. Using the large virtual-target definition resulted in twice as many false-positive feeders compared with the medium virtual-target definition. The use of AFD software with a medium virtual target may offer an optimal balance between high sensitivity and an acceptable number of false-positive feeders. This approach may enhance the potential clinical benefits of using AFD software, including reduced procedure time, decreased radiation exposure, and improved technical success, as reported in studies on AFD-assisted transarterial chemoembolization for HCC [10-12].

The delineation of the virtual target is a key step in the use of AFD software. The virtual target is delineated manually by an operator or radiological technologist, and differences in the target definition may cause variability in the feeders identified by the software. Nevertheless, little has been reported on how the virtual target definition affects feeder detection performance. Iwazawa et al. [8] evaluated the feeder detectability of the AFD software in transarterial chemoembolization of HCC across three different virtual-target settings. The feeder-detection sensitivities of the small, medium, and large target protocols were 79.8%, 91.7%, and 96.3%, respectively; the specificities were 95%, 88%, and 50%, respectively; and the overall accuracies were 87.5%, 89.9%, and 74%, respectively [8]. The findings indicate that a medium-sized target, which includes the entire

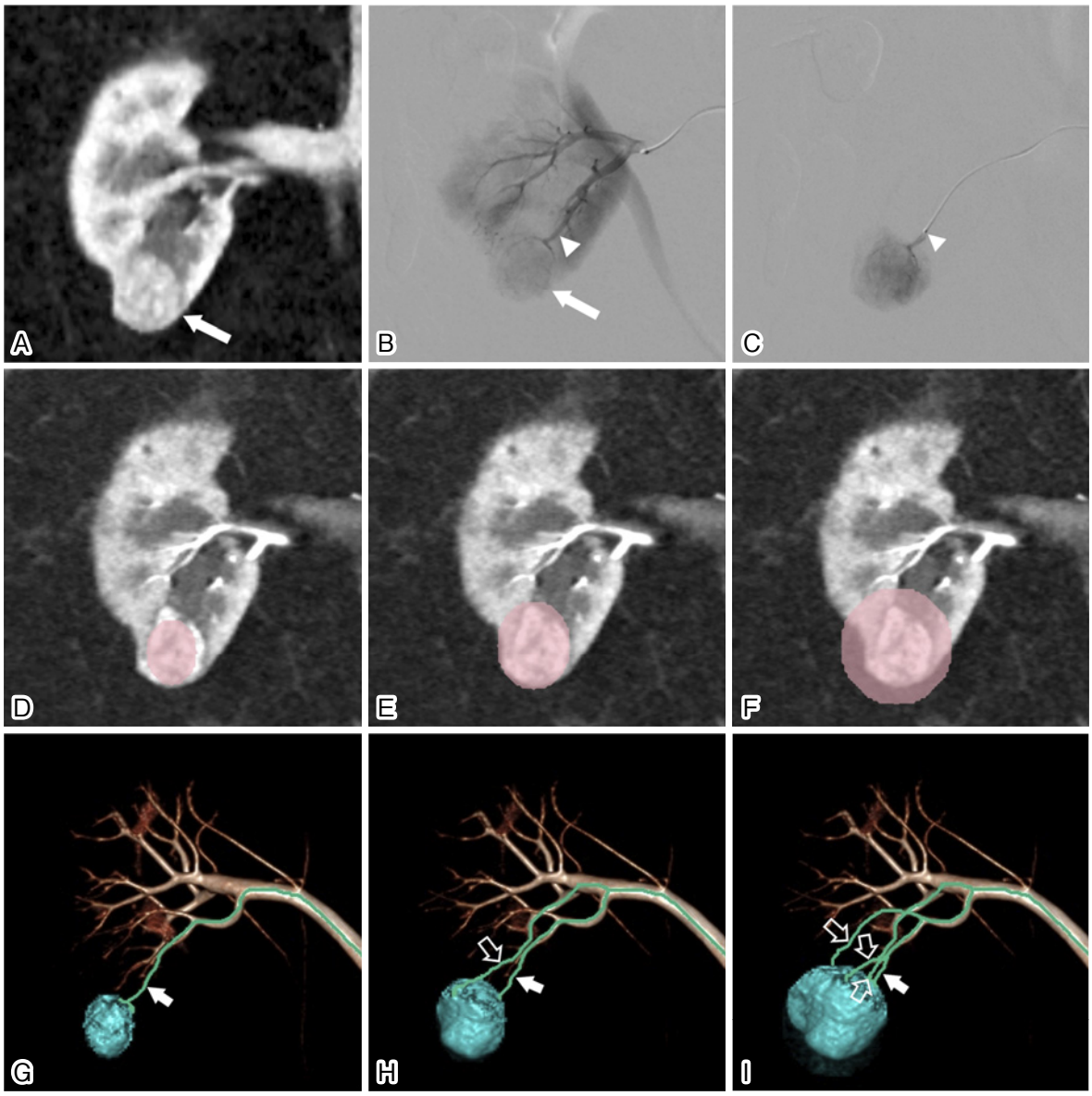

Figure 3. Images of right renal cell carcinoma.
(A) Preprocedural contrast-enhanced CT demonstrates a 25-mm renal cell carcinoma in the right kidney (arrow). (B) Selective digital subtraction angiography performed via a microcatheter demonstrating tumor staining (arrow). The arrowhead indicates a distal arterial branch corresponding to the tumor feeder. (C) Selective digital subtraction angiography from the tumor feeder. The arrowhead indicates the position of the microcatheter tip, from which the ethiodized oil was injected. (D, E, F) Coronal CT images showing delineation of the virtual targets (D: small, E: medium, and F: large). (G, H, I) Demonstration of potential tumor feeders by automated feeder-detection software using the three virtual-target definitions (G: small, H: medium, and I: large). True-positive (solid arrows) and false-positive (hollow arrows) feeders are shown in the images.

tumor without an additional peripheral margin, may yield the most accurate feeder detection in HCC. Similarly, the present study confirms that the medium virtual-target definition is effective for software-based feeder detection in RCC.

The increase in false-positive feeders with a larger virtual target in the present study is consistent with the findings of Iwazawa et al. [8]. This is likely because AFD software may detect arteries that supply the normal renal parenchyma surrounding the tumor as potential feeders when using large virtual targets. In contrast, the low sensitivity (48.0%) of the large virtual target in our study contradicted the findings of the previous study, which showed high sensitivity with a large target definition [8]. This discrepancy may be attributed to differences in organ types and software algorithms. In addition, our strict criterion for classifying true-positive feeders may have contributed to the low sensitivity of the large virtual-target definition. We classified a software-detected vessel as a true positive only when the software demonstrated the entire vessel course up to the distal branch into which the ethiodized oil was injected, aiming to thoroughly assess the software's ability to identify the specific arterial branches that need to be selected by a microcatheter for ethiodized-oil injection. Accordingly, partial detection of the feeder vessel, which occurred when the distal arterial

Table 1. Patient and Tumor Characteristics.

Patients (n = 17)		Tumors (n = 17)	
Age (years), mean ± SD	68.8 ± 10.5	Diameter (mm), mean ± SD	25.6 ± 10.1
Sex, male/female (%)	14/3 (82.4/17.6)	Histology, clear cell/unclassified (%)	15/2 (88.2/11.8)
BMI (kg/m^2), mean ± SD	25.5 ± 4.3	Laterality, right/left (%)	11/6 (64.7/35.3)
eGFR (mL/min/1.73m^2), mean ± SD	61.8 ± 17.1	Location, exophytic/mixed (%)	11/6 (64.7/35.3)
		Number of feeding arteries per tumor, single/dual/triple (%)	12/2/3 (70.6/11.8/17.6)

BMI: body mass index; eGFR: estimated glomerular filtration rate; SD: standard deviation

Table 2. Feeder-Detection Sensitivity and Number of False-Positive Feeders per Tumor When Using Automated Feeder-Detection Software with Three Virtual-Target Definitions for Renal Cell Carcinoma.

Detection performance metrics	Virtual-target definitions		
	Small	Medium	Large
Sensitivity*, %	80.0 (20/25)	88.0 (22/25)	48.0 (12/25)
Number of false-positive feeders per tumor, mean ± SD	0.82 ± 1.3	1.41 ± 1.1	2.82 ± 1.6

*Sensitivity was calculated by dividing the number of true-positive feeders by the total number of treated feeders.
SD: standard deviation

branch was covered by the large virtual target area, was excluded from true positives. Such a definition of a true positive may differ from that used in the previous study, which identified true positives based on angiography findings but did not specify whether the software was able to visualize the most distal treated branch [8]. Unlike chemoembolization for HCC, in which both the tumor and surrounding margins are often included in the treatment area to achieve a complete response, the surrounding margin is not intentionally included in the treatment area in ethiodized-oil marking for RCC. Thus, we typically advance the microcatheter into the distal arterial branches as close to the tumor as possible, aiming to minimize renal damage resulting from ethiodized oil injection into the normal renal parenchyma. Consequently, the distal arterial branches selected by the microcatheter may be in close proximity to the tumor and potentially encompassed in the area of the virtual target if a large virtual target definition is employed.

This study has some limitations. First, this was a retrospective study with a small sample size. Second, the findings obtained in this study cannot be directly applied to different AFD software programs because the feeder-detection algorithms vary. Third, this study used a 320-row area-detector CT scanner, which allowed volume scanning of the entire kidney with high temporal resolution and high-contrast renal CTA with minimal cortical enhancement. Although such imaging is considered preferable for software-based feeder detection, it may not be replicable when conventional CT scanners are used. Fourth, although ellipsoidal segmentation—rather than freeform contouring—was adopted to enhance reproducibility, manual delineation of the virtual target may still introduce inter-operator variability, potentially compromising the generalizability of the study results.

Conclusion

The RCC feeder-detection rate with the AFD software varies according to the virtual-target definitions. The medium virtual-target definition, that is, covering the entire tumor with a minimal peripheral margin, may provide the highest feeder-detection sensitivity, with an acceptable number of false-positive feeders.

Acknowledgement: We sincerely thank Akira Kurozumi for his contribution to the image analysis. ChatGPT, DeepL, Grammarly, and Paperpal were used for English editing in the manuscript preparation process, and the validity of all text was thoroughly confirmed by the authors. We would also like to thank Editage (www.editage.jp) for the English editing.

Author Contributions: Conceived and designed the study: YM, TK, SO
Data collection and analysis: TK, SO
The first draft of the manuscript was written by: SO, YM
Contributed to revising previous versions of the manuscript: all authors
Approved the final manuscript: all authors

Conflicts of Interest: YM received a grant and a lecturer's fee from Canon Medical Systems outside the submitted work. TH received a grant from Canon Medical Systems outside the submitted work. The other authors have no relevant conflicts of interest to disclose.

Clinical Registration Number: None

Ethical Approval: This study was approved by the Institutional Review Board (approval number: ken2211-035). All procedures performed in this study were in accordance with

the ethical standards of the institutional and/or national research committee and with the 1964 Helsinki declaration and its later amendments or comparable ethical standards.

The preliminary version of this study was presented at the 53rd Annual Meeting of the Japanese Society of Interventional Radiology. One tumor without a pathological diagnosis was excluded in the current version. The current version involved the validation of image analysis by two evaluators.

References

1. Gobara H, Matsui Y, Uka M, et al. Percutaneous cryoablation combined with prior transcatheter arterial embolization for renal cell carcinomas of 3 cm or larger: a prospective study. Int J Clin Oncol. 2022; 27: 1589-1595.
2. Winokur RS, Pua BB, Madoff DC. Role of combined embolization and ablation in management of renal masses. Semin Intervent Radiol. 2014; 31: 82-85.
3. Miller JM, Julien P, Wachsman A, Van Allan RJ, Friedman ML. The role of embolization in reducing the complications of cryoablation in renal cell carcinoma. Clin Radiol. 2014; 69: 1045-1049.
4. Tsuji Y, Miura H, Hirota T, et al. Transarterial ethiodised oil marking before CT-guided renal cryoablation: evaluation of tumour visibility in various renal cell carcinoma subtypes. Clin Radiol. 2023; 78: 279-285.
5. Kubo T, Arai Y, Sone M, et al. Detectability of feeding arteries using automated feeding artery detection software based on CT arteriography in transarterial embolisation. Singapore Med J. 2022; 10.11622/smedj.2022060.
6. Cui Z, Shukla PA, Habibollahi P, Park HS, Fischman A, Kolber MK. A systematic review of automated feeder detection software for locoregional treatment of hepatic tumors. Diagn Interv Imaging. 2020; 101: 439-449.
7. Matsui Y, Tomita K, Uka M, et al. Automated feeder-detection software for renal cell carcinoma embolization: A retrospective evaluation of detection rate using transarterial time-resolved computed tomography angiography. Cardiovasc Intervent Radiol. 2024; 47: 132-138.
8. Iwazawa J, Ohue S, Hashimoto N, Mitani T. Accuracy of software-assisted detection of tumour feeders in transcatheter hepatic chemoembolization using three target definition protocols. Clin Radiol. 2014; 69: 145-150.
9. Kanda Y. Investigation of the freely available easy-to-use software 'EZR' for medical statistics. Bone Marrow Transplant. 2013; 48: 452-458.
10. Iwazawa J, Ohue S, Hashimoto N, Mitani T. Comparison of the number of image acquisitions and procedural time required for transarterial chemoembolization of hepatocellular carcinoma with and without tumor-feeder detection software. Radiol Res Pract. 2013; 2013: 580839.
11. Miyayama S, Yamashiro M, Sugimori N, Ikeda R, Okimura K, Sakuragawa N. Outcomes of patients with hepatocellular carcinoma treated with conventional transarterial chemoembolization using guidance software. J Vasc Interv Radiol. 2019; 30: 10-18.
12. Miyayama S, Yamashiro M, Nagai K, Tohyama J, Kawamura K. Efficacy of automated tumor-feeder detection software using cone-beam computed tomography technology in transarterial targeted therapy. Interv Radiol (Higashimatsuyama). 2016; 1: 28-38.